AGU PUBLICATIONS

Geophysical Research Letters

RESEARCH LETTER
10.1002/2015GL065452

Key Points:
- The first observation of Pi2-like pulsations during Mercury's substorm
- Alfvénic and compressional waves were observed in the different regions of the plasma sheet
- We proposed the sources for the plasma waves

Correspondence to:
W.-J. Sun,
weijiesun@pku.edu.cn

Citation:
Sun, W.-J., et al. (2015), MESSENGER observations of Alfvénic and compressional waves during Mercury's substorms, *Geophys. Res. Lett.*, *42*, 6189–6198, doi:10.1002/2015GL065452.

Received 20 JUL 2015
Accepted 27 JUL 2015
Accepted article online 30 JUL 2015
Published online 14 AUG 2015

MESSENGER observations of Alfvénic and compressional waves during Mercury's substorms

Wei-Jie Sun[1,2], James A. Slavin[2], Suiyan Fu[1], Jim M. Raines[2], Torbjörn Sundberg[3], Qiu-Gang Zong[1], Xianzhe Jia[2], Quanqi Shi[4], Xiaochen Shen[4], Gangkai Poh[2], Zuyin Pu[1], and Thomas H. Zurbuchen[2]

[1]School of Earth and Space Sciences, Peking University, Beijing, China, [2]Department of Atmospheric, Oceanic and Space Sciences, University of Michigan, Ann Arbor, Michigan, USA, [3]School of Physics and Astronomy, Queen Mary University of London, London, UK, [4]Shandong Provincial Key Laboratory of Optical Astronomy and Solar-Terrestrial Environment, School of Space Science and Physics, Shandong University, Weihai, China

Abstract MErcury Surface, Space ENviroment, GEochemistry, and Ranging (MESSENGER) magnetic field measurements during the substorm expansion phase in Mercury's magnetotail have been examined for evidence of low-frequency plasma waves, e.g., Pi2-like pulsations. It has been revealed that the B_y fluctuations accompanying substorm dipolarizations are consistent with pulses of field-aligned currents near the high-latitude edge of the plasma sheet. Detailed analysis of the B_y fluctuations reveals that they are near circularly polarized electromagnetic waves, most likely Alfvén waves. Soon afterward the plasma sheet thickened and MESSENGER detected a series of compressional waves. These Alfvénic and compressional waves have similar durations (10–20 s), suggesting that they may arise from the same source. Drawing on Pi2 pulsation models developed for Earth, we suggest that the Alfvénic and compressional waves reported here at Mercury may be generated by the quasi-periodic sunward flow bursts in Mercury's plasma sheet. But because they are observed during the period with rapid magnetic field reconfiguration, we cannot fully exclude the possibility of standing Alfvén wave.

1. Introduction

Substorms are energy circulation and dissipation processes which are initiated in the nightside magnetosphere and accompanied by a number of phenomena, such as Pi2 pulsations, auroral intensifications, energetic particle injections, and ejection of plasmoids, etc. [e.g., *Akasofu*, 1964; *Hones*, 1977; *Baker et al*., 1996; *Olson*, 1999; *Slavin et al*., 2002]. One of the key elements is the substorm current wedge (SCW), which provides coupling between the magnetosphere and the ionosphere [e.g., *McPherron et al*., 1973; *Birn et al*., 1999; *Yao et al*., 2012; *Kepko et al*., 2014]. Pi2 pulsations are irregular ultralow frequency wave events with periods from 40 to 150 s and short durations of ~10 to 15 min. They are believed to be an integral part of the SCW [e.g., *Baumjohann and Glaßmeier*, 1984; *Keiling and Takahashi*, 2011]. Extensive research has revealed a close relationship between high-latitude Pi2 pulsations and the formation of the SCW, both of which are intimately related to flow bursts in the plasma sheet [e.g., *Lester et al*., 1983; *Baumjohann and Glaßmeier*, 1984; *Olson*, 1999; *Keiling and Takahashi*, 2011; *Hsu et al*., 2012].

Mariner 10 observed possible substorm dipolarizations during its flybys of Mercury, which were accompanied by energetic electrons (>35 keV) [*Baker et al*., 1986; *Christon et al*., 1987; *Slavin et al*., 1997]. The MErcury Surface, Space ENviroment, GEochemistry, and Ranging (MESSENGER) [*Solomon et al*., 2007] have observed dipolarization fronts (DFs) which are indirect evidence of reconnection-driven flow bursts in the plasma sheet [*Sundberg et al*., 2012]. The MESSENGER magnetic field measurements have also revealed several minute long tail loading-unloading events which appear to be Mercury analogues to the growth and expansion phases observed an ~1 to 2 h time scales during substorms at Earth [*Slavin et al*., 2010, 2012]. Recently, *Sun et al*. [2015] reported the detailed observations of substorm activity in Mercury's near magnetotail. They found that the plasma sheet thins during these apparent substorm growth phases and then, just like at Earth, suddenly thickens as magnetic field relaxes into a more dipolar configuration during the expansion phase.

These observations of so many familiar substorm phenomena beg the question "does Mercury have an analogue to the Pi2 pulsations observed near substorm expansion onset at Earth?" There are many different Pi2 pulsation models for Earth's magnetosphere, including plasmaspheric cavity resonance, drift ballooning wave, bouncing Alfvén waves, modulated flow bursts braking, and plasma sheet interchange oscillations, etc. [see *Keiling and Takahashi*, 2011; *Wolf et al*., 2012]. We know that Mercury's magnetosphere is different from

the Earth's magnetosphere in some key aspects, such as the lack of a conducting ionosphere or a plasmasphere [e.g., *Ip*, 1986; *Glassmeier*, 2000; *Slavin et al*., 2007; *Lyatsky et al*., 2010]. It is exactly because of these differences that the study of plasma waves during Mercury's substorms is very meaningful. The examination of such waves under the unique conditions found at Mercury may help us to better understand and appreciate the formation of SCW and the sources for Pi2 pulsations at Earth.

In this work, we report the first observations of Alfvénic and compressional waves during substorm expansion phase at Mercury. The Alfvén waves are believed to be the carriers for pulses of field-aligned current which communicate changes in magnetotail configuration during substorm dipolarization events to Mercury's nightside polar region. We propose that these wave activities may be Mercury analogues to Earth's Pi2 pulsations. Comparison of the existing Pi2 models for Earth with these MESSENGER observations suggests that these Mercury wave events are most likely generated by the braking of quasi-periodic flow bursts in the near tail [*Kepko et al*., 2001]. However, we cannot fully exclude the possibility that they might be standing Alfvén waves.

2. Observations

Our study is based upon the MESSENGER magnetic field data (20 samples per second) and low-energy proton data (10 s energy scan from 50 eV/q to 13 keV/q) provided by the Magnetometer [*Anderson et al*., 2007] and the Fast Imaging Plasma Spectrometer sensor (FIPS) [*Andrews et al*., 2007], respectively. The magnetic field is analyzed in Mercury Solar Magnetospheric (MSM) coordinates. In this coordinate system, X_{MSM} and Y_{MSM} are in Mercury's magnetic equatorial plane, which is displaced ~0.2 R_M northward from Mercury's geographic equator. X_{MSM} is sunward, and Z_{MSM} is normal to the magnetic equatorial plane and positive northward. Y_{MSM} completes this right-handed coordinate system. The spacecraft location is given in an aberrated coordinates system (MSM') for the MSM X and Y axes have been rotated, so that the average solar wind flow is antiparallel to X'_{MSM}.

2.1. Case I

Figure 1 shows the overview of a substorm event at Mercury (Case I) with clear plasma sheet thinning and thickening features [*Sun et al*., 2015]. This event was observed by MESSENGER between 1611:00 and 1617:00 UT on 9 December 2012. The plasma sheet thinning during the substorm growth phase is identified between the first and second vertical dashed lines for the almost constant B_x (Figure 1c, red curve), decrease in B_z (Figure 1e), and small increase in $|B_y|$ (Figure 1d). The plasma sheet thickening during the substorm expansion phase is defined between the second and third vertical dashed lines with a substorm dipolarization (sharp increase in B_z and was followed by a sharp decrease in B_x) as the initiation. There were two B_y pulses (indicated by the two red arrows in Figure 1d) near the substorm dipolarization, and they were followed by a series of perturbations in B_x and the total magnetic field intensity (B_t) (Figure 1c). In order to see the field perturbations clearly, the magnetic field data points were continuously subtracted by the background magnetic field, which is the averaged field within ±15 s interval on either side of each point. Figures 1f and 1g show the perturbations of total magnetic field (δB_t) and three magnetic field components (δB_x, δB_y, δB_z), respectively. Figure 1h shows the magnetic field fluctuations (δB_{para}, δB_{perp1}, δB_{perp2}) in a field-aligned coordinate system, where B_{para} is along the background magnetic field, B_{perp1} is perpendicular to the plane of B_{para} and X_{MSM}, and B_{perp2} completes the right-handed coordinate system.

Near the substorm onset indicated by dipolarization, the magnetic field is mainly the B_x (Figure 1c), so that J_x would be the primary contributor to $J_{||}$. Therefore, the two B_y pulses marked by the red arrows in Figure 1d could be the signature of field-aligned currents (FACs) according to Ampère's law. The time profiles of δB_z for the two pulses are bipolar, while δB_y and δB_x are unipolar (Figure 1g). And under the field-aligned coordinates, δB_{perp1} is unipolar with δB_{perp2} bipolar for the first pulse and δB_{perp1} is bipolar with δB_{perp2} unipolar for the second pulse (Figure 1h), which agrees with the signature of electromagnetic pulses [e.g., *Parks et al*., 2007]. We have applied the minimum variance analysis (MVA) [*Sonnerup and Scheible*, 1998] on them. The MVA results and hodograms for both events are shown in Figures 1i and 1j. The maximum eigenvalues (λ_{max}) for both events are close ($\lambda_{max}/\lambda_{int} < 3$) to the intermediate eigenvalues (λ_{int}), but they are much larger ($\lambda_{int}/\lambda_{min} > 20$) than the minimum eigenvalues (λ_{min}). This is the expected result when applying MVA to a planar wavefront [*Sonnerup and Scheible*, 1998]. The minimum variance direction n_{min}, which is the wave vector (or **k**) [*Sonnerup and Scheible*, 1998; *Parks et al*., 2007], for the first B_y pulse is ± (0.65, −0.45, 0.61). It corresponds

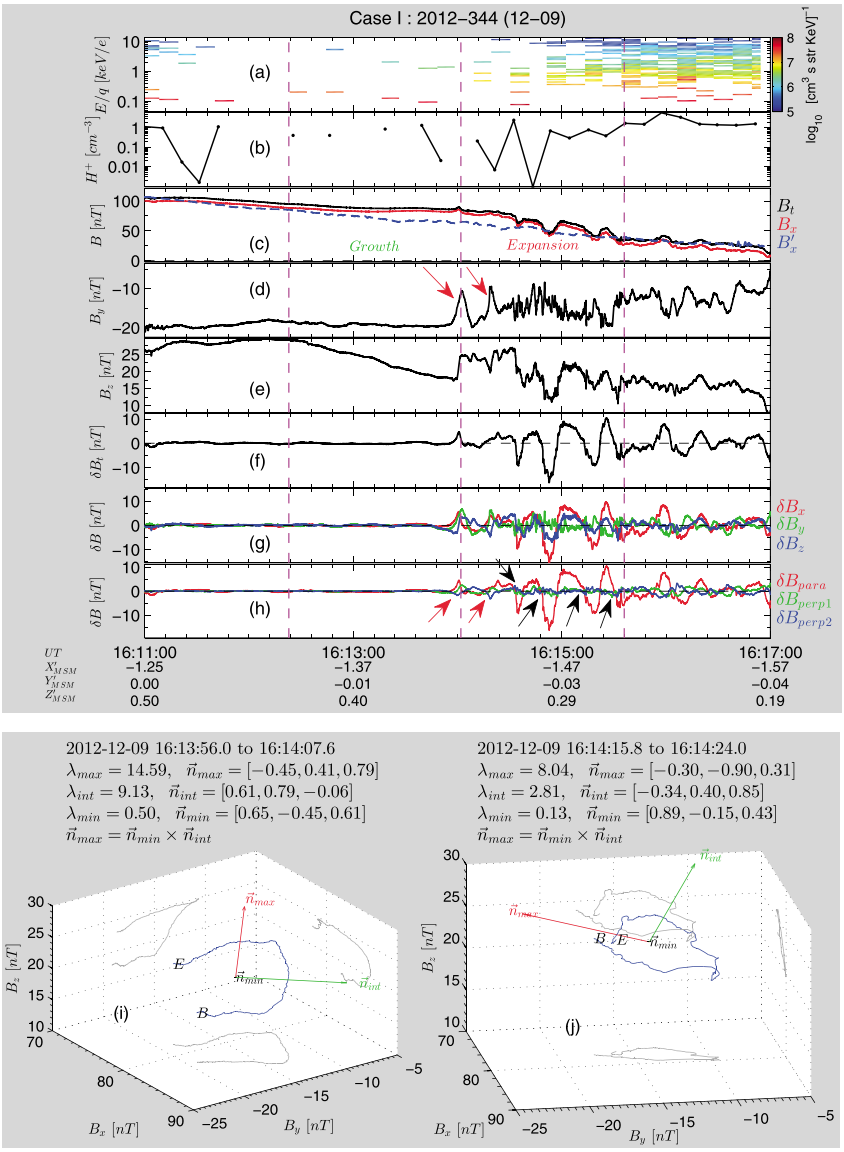

Figure 1. (a) Energy spectrum for proton differential particle flux, (b) the observed proton density, (c) B_t (black), B_x (red), B_x' (blue), (d) B_y, (e) B_z, (f) δB_t, (g) δB_x (red), δB_y (green), δB_z (blue), (h) δB_{para} (red), δB_{perp1} (green), δB_{perp2} (blue). B_x' represents the magnetic field measurement from the nearest nonsubstorm plasma sheet crossing. The first, second, and third vertical dashed lines indicate the beginning of loading phase, expansion phase, and recovery phase. (i) Hodogram of the magnetic vectors from 1613:56.0 to 1614:07.6 UT and (j) hodogram of the magnetic vectors from 1614:15.8 to 1614:24.0 UT. The hodograms are in the plane normal to minimum variance vector (n_{min}), the red arrow indicates the maximum variance direction (n_{max}), and green arrow indicates the intermediate variance direction (n_{int}), the beginning and end of the trace are marked with *B* and *E*.

to ~ 38° (or ~ 142°) from the background B. The **k** vector for the second pulse is ± (0.89, −0.15, 0.43) and is ~ 9° (or ~ 171°) from the background B. In the plane normal to **k** (the hodograms in Figures 1i and 1j), the magnetic field vectors rotated circularly by ~ 360° with the durations of ~ 11 s and ~ 10 s for the two pulses, respectively. To summarize, the two B_y pulses near substorm onset, which are the signatures of field-aligned current, are circularly polarized electromagnetic waves and propagate nearly parallel (or antiparallel) to the background magnetic field. We conclude that they are probably Alfvén wave pulses. However, it is worth noticing that these pulses are not purely transverse waves, they also have a component parallel to the background magnetic field (Figure 1h). Following the two Alfvénic pulses, four successively compressional waves marked by the black arrows in Figure 1h were observed before the end of plasma sheet thickening process. The compressional waves are distinguished by the fluctuations in δB_t (Figure 1f) and the large compressional component (δB_{para} in Figure 1h).

The two Alfvénic pulses were observed at the start of plasma sheet thickening. The small observed proton number density ($<0.1\,cm^{-3}$, Figure 1b) [*Raines et al*., 2013] and the high Z'_{MSM} (~0.35 R_M) suggest that MESSENGER was near the high-latitude edge of the plasma sheet during that time. But MESSENGER detected high observed proton densities (~1 cm^{-3}) when compressional waves appeared indicating that the spacecraft had moved into the inner plasma sheet. The durations of the two Alfvénic and four compressional waves are ~ 11 s, ~ 10 s, ~ 12 s, ~ 19 s, ~ 24 s, and ~ 12 s, respectively. We note that these values are similar to the durations of flow bursts observed in Mercury's plasma sheet (~10 s on average) by *Sundberg et al*. [2012]. Flow bursts in the Earth's plasma sheet generally have higher magnetic field and lower plasma density than the ambient plasma sheet with a leading edge of DF [e.g., *Chen and Wolf*, 1993; *Sergeev et al*., 1996; *Ohtani et al*., 2004; *Liu et al*., 2013, 2014; *Sun et al*., 2014]. For this reason, it may be assumed that the durations of the higher magnetic field region in *Sundberg et al*. [2012] are indicators of the duration of flow bursts.

2.2. Case II

Figure 2 shows another event (Case II) observed by MESSENGER between 1536:00 and 1541:30 UT on 22 June 2012. Similar to Figure 1, the three vertical dashed lines indicate the onset of plasma sheet thinning, plasma sheet thickening, and the end of plasma sheet thickening, respectively, from left to right. This event also possessed two B_y pulses (Figure 2d) around the time of substorm dipolarization. We employed the same method as in Figure 1 to obtain the magnetic perturbation fields. For the first pulse, the time profile of δB_{perp2} is bipolar with δB_{perp1} unipolar (the first red arrow in Figure 2h). Its normal direction **k** is ± (0.43, −0.46, 0.78) which is ~ 31° or ~ 149° from the background B, and the λ_{max} and λ_{int} are close to each other (~5) but much larger (~47) than λ_{min}. And in the plane normal to **k**, magnetic field vectors rotated circularly by ~ 270° (Figure 2i). The above features of the first pulse also indicate it is an Alfvén wave pulse. But the second pulse is different from the first pulse in some features (the second red arrow in Figure 2h). The MVA eigenvalue ratios ($\lambda_{max}/\lambda_{int}$ ~ 3 and $\lambda_{int}/\lambda_{min}$ ~ 34) are still consistent with the planar wavefront feature. But **k** (± (−0.55, −0.20, 0.81)) is almost perpendicular (~90°) to the background B. And in the plane normal to **k**, magnetic field vectors rotated elliptically (Figure 2j). It seems that the second pulse still has the electromagnetic wave signature, but it may not be a transverse wave. After the two pulses, MESSENGER also observed a series of compressional waves (marked by the black arrows in Figure 2h), which are mainly in the field-aligned component (δB_{para}) and correspond with the fluctuation of δB_t (Figure 2f).

For this event, the two electromagnetic pulses were also observed at the beginning of plasma sheet thickening. Thus, they were located nearer the edge of the plasma sheet than the compressional waves observed subsequently. This is similar to the wave locations for Case I. The durations for the electromagnetic pulses and compressional waves are ~ 11 s, ~ 10 s, ~ 10 s, ~ 11 s, ~ 14 s, ~ 10 s, and ~ 13 s, respectively, which are also similar to the early case and the durations expected for flow bursts at Mercury [*Sundberg et al*., 2012].

3. Sources for the Plasma Waves

The observations of Alfvén wave pulses in association with substorm dipolarizations in both of our Mercury cases support the idea that changes in magnetospheric configuration are communicated to the ionosphere and surface of the Mercury, respectively, via field-aligned currents carried by Alfvén waves [e.g., *Southwood and Kivelson*, 1991; *Kepko et al*., 2014]. It is also consistent with the concept that the formation of SCW after the substorm expansion onset starts out as Alfvén waves propagating along the magnetic field line toward the nightside polar region [e.g., *Baumjohann and Glaßmeier*, 1984; *Kepko et al*., 2014].

The Alfvénic and compressional waves observed during the substorm expansion phase analyzed in both cases reveal quasi-periodic features, similar to Pi2 pulsations at Earth [e.g., *Baumjohann and Glaßmeier*, 1984; *Keiling and Takahashi*, 2011]. For this reason, we call these waves "Pi2-like pulsations" at Mercury. The Pi2-like pulsations at Mercury were detected during the whole substorm expansion phase (~1 min) similar to the Pi2 wave packets that are also observed throughout the expansion phase at Earth [e.g., *Keiling and Takahashi*, 2011]. But these Pi2-like pulsations possess shorter periods (10–20 s) than that of Earth, which are from 40 to 150 s.

3.1. Pi2 Models at Earth

As mentioned in section 1, many models have been proposed for Pi2 pulsations during substorm at Earth, including plasmaspheric cavity mode [e.g., *Southwood and Kivelson*, 1990; *Lin et al*., 1991], ballooning waves

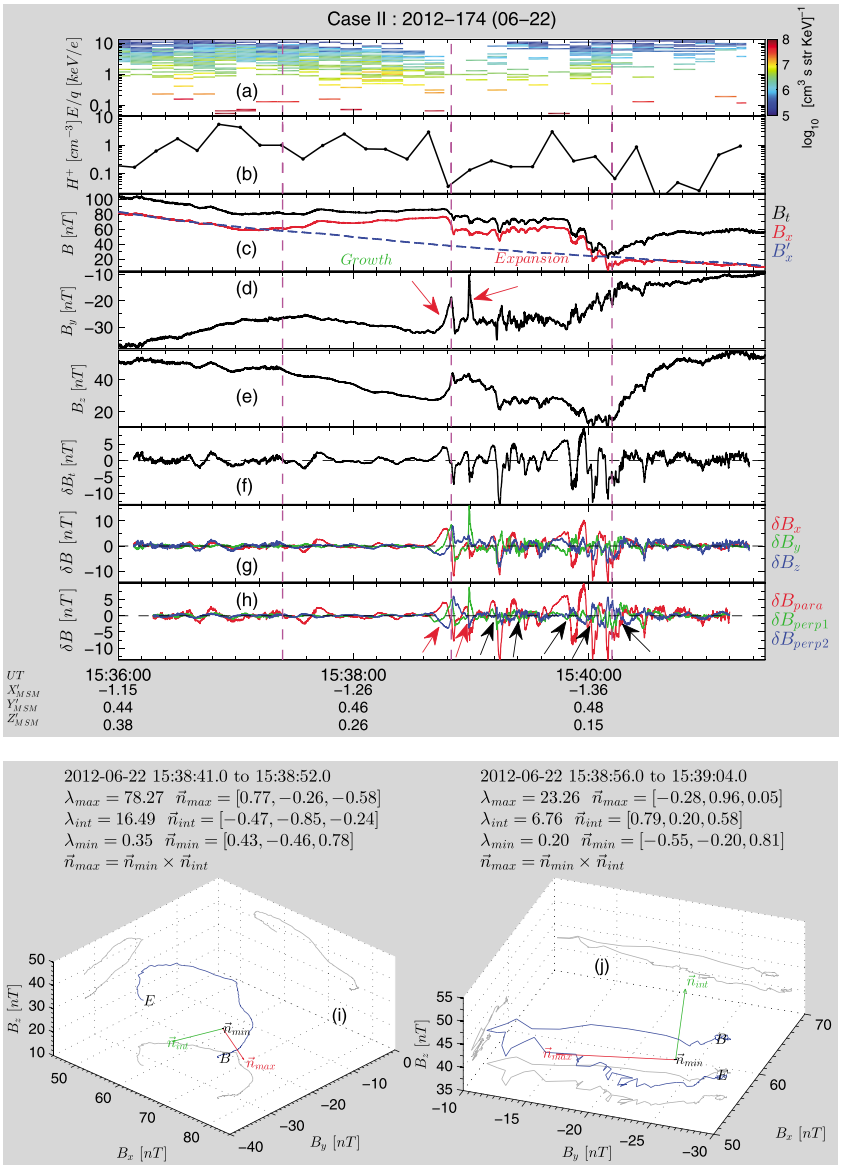

Figure 2. The figure is in the same format of Figure 1.

[*Solovyev et al.*, 2000; *Keiling*, 2012], bouncing Alfvén waves [e.g., *Maltsev et al.*, 1974; *Lester et al.*, 1983; *Baumjohann and Glaßmeier*, 1984], interchange oscillations in the plasma flow [*Wolf et al.*, 2012; *Keiling et al.*, 2014; *Panov et al.*, 2014], and the braking of quasi-periodic flow bursts in the plasma sheet [*Kepko and Kivelson*, 1999; *Kepko et al.*, 2001]. Mercury is a very slow rotating planet (i.e., rotation period of ~58.6 days). If it had one, Mercury's plasmasphere would be located inside ~0.02 R_M [*Glassmeier*, 1997]. Therefore, models requiring a plasmaspheric cavity are ruled out, such as the plasmaspheric cavity resonance and ballooning waves occurring at the inner edge of plasma sheet.

3.2. Standing Alfvén Waves

Some studies have proposed that the formation of SCW at Earth starts out as Alfvén waves launched by the flow bursts braking process and propagating toward the high-latitude ionospheres. The Alfvén wave would bounce back and forth between the two hemispheres due to the mismatch of impedance between the wave and ionosphere, and they are believed to give rise to at least some of the ground high-latitude Pi2 pulsations

[*Baumjohann and Glaßmeier*, 1984; *Keiling and Takahashi*, 2011]. In this model, the period of the Pi2 pulsation is the Alfvén wave travel time between the north and south hemispheres

$$\tau_{AT} = 2\int_{NH}^{SH} dl_{||}/v_A(l_{||})$$

where v_A is the Alfvén speed and the integration is along the magnetic field line from north hemisphere (NH) to south hemisphere (SH). To estimate the τ_{AT} for our events, we have employed the Mercury magnetosphere model developed by *Alexeev et al.* [2008, 2010], see also *Johnson et al.* [2012] to obtain the length of magnetic field line and the field magnitude along the field line. The lengths of the magnetic field lines for the two events in Cases I and II are ~ 2.2 R_M and ~ 1.5 R_M, respectively. Because we cannot obtain the plasma density along the entire field line, we have assumed two values (0.5 and 3 cm^{-3}) for the averaged proton number density, and assumed sodium to be present with a number density ~ 10% that of the protons, based upon the average plasma sheet composition obtained from FIPS [*Gershman et al.*, 2014]. The estimated τ_{AT} is 5.0–10.5 s and 2.5–5.5 s for the two cases, respectively, which are about half the period of the observed Alfvén waves (10–20 s) in our events. But we have to note that the lengths of the magnetic field lines are highly dependent on magnetosphere conditions, especially during reconnection-driven loading and unloading periods of the tail, i.e., our cases [*Slavin et al.*, 2010, 2012; *Sun et al.*, 2015]. Therefore, the τ_{AT} would vary greatly with a wider range than our estimation. But because of the limited conductivity of the regolith in Mercury's surface [e.g., *Verhoeven et al.*, 2009; *Anderson et al.*, 2014; *Jia et al.*, 2015], the waveform of the bouncing Alfvén wave should be damped and sinusoidal [e.g., *Glassmeier*, 1997], which is not the case for our events. However, given the rapid magnetic field lines reconfiguration taking place during these events, we cannot rule out the possibility that standing Alfvén waves are the source of these events.

If we took a look closely to the Case I after the two Alfvénic pulses in Figure 1d, there are some B_y fluctuations with smaller periods than the Alfvénic and compressional waves. Figure 3 shows a further analysis between 1614:20 and 1615:10 UT on these fluctuations. The periodic B_y fluctuations were observed during the compressional waves (Figure 3a), and the wavelet power spectrum (Figure 3b) gives a period of ~ 2–5 s for them, which is the enclosed region by contour with greater than 95% confidence level [*Torrence and Compo*, 1998]. Band-pass filtered (from 2 to 5 s) δB_x, δB_y, and δB_z (Figures 3c–3e) show that most of the waves during this duration have the signature of the electromagnetic waves, which is that the peaks of δB_y correspond with the bipolar of δB_x or (and) δB_z. In contrast with the longer period (~10–20 s) waves, the ~ 2–5 s period waves seem consistent with the predicted value for standing Alfvén wave. Absent more detailed measurements (e.g., electric fields), the wave pulses are suggestions of standing Alfvén waves but not definitive. For Case II, we do not observe this shorter period plasma waves during the substorm expansion phase.

3.3. Interchange Oscillations

Recently, some researchers proposed that the interchange oscillations of the plasma flow near the flow braking region could also produce Pi2 pulsation [*Wolf et al.*, 2012; *Keiling et al.*, 2014; *Panov et al.*, 2014]. There are two features of this type of Pi2 pulsation. One is that the waveforms show sharp peaks (i.e., narrow bandwidth) in one direction. The other is that the wave amplitudes decay with time. For both of our events, the wave amplitudes are asymmetric and independent of time, which is quite different from the expectations for interchange oscillations. Thus, the interchange oscillations could be ruled out as the source for our cases.

3.4. Quasi-Periodic Flow Bursts

There is one model for which Pi2 pulsations are driven by quasi-periodic flow bursts in the plasma sheet, i.e., each flow burst drives one single Pi2 pulse [*Kepko and Kivelson*, 1999; *Kepko et al.*, 2001]. In this model, the flow bursts and Pi2 pulsations are predicted to be of similar duration and amplitude. We suggest that our events are most consistent with this mechanism for the following reasons. First, although we cannot directly observe the flow bursts with only one spacecraft (in fact, we cannot detect plasma flows due to FIPS's field of view), the wave event durations are similar to those of the sunward moving flow bursts derived from analysis of near-tail DFs [*Sundberg et al.*, 2012]. Second, the durations (~10–20 s) of Alfvénic and compressional waves are in the same temporal range, indicating that they may arise from the same source. Further, *Kepko et al.* [2001] described the propagation paths for different waves generated by flow bursts. One is a fast-mode wave that propagates toward the planet in the equatorially confined nightside region. Another is the Alfvén wave carrying field-aligned current that propagates toward the nightside polar region. In this scenario,

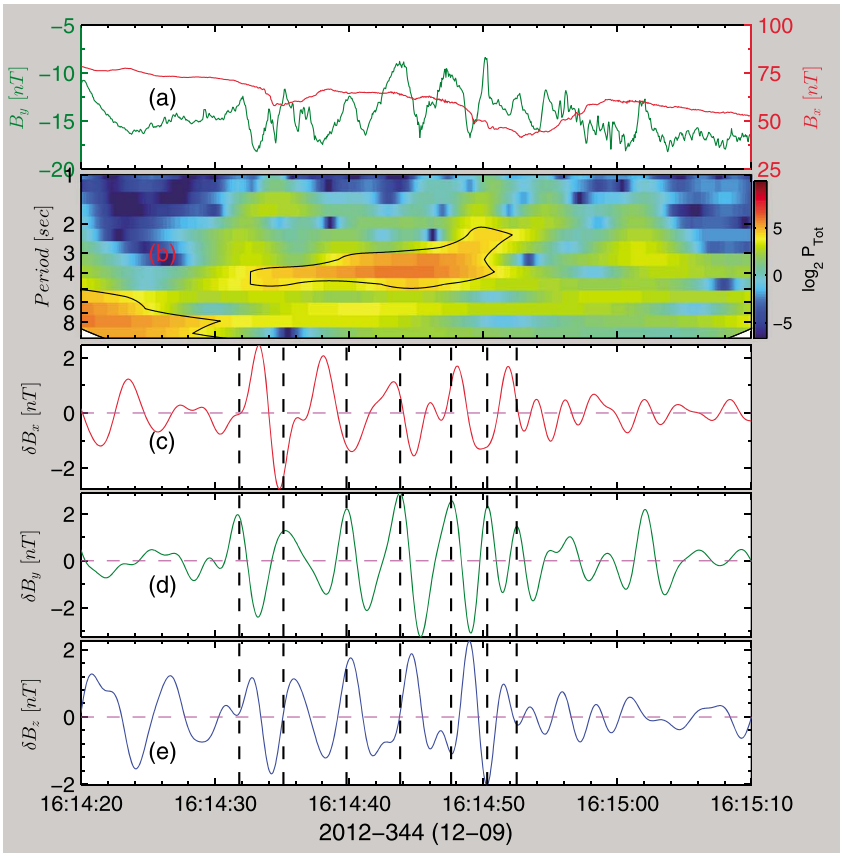

Figure 3. (a) B_y (green) and B_z (red), (b) wavelet power spectrum of B_y, the contour encloses region of 95% confidence level, (c–e) band-pass filtered (2–5 s) magnetic field data for the three components. Vertical dashed lines mark each peak of δB_y.

one would detect Alfvén waves in the off-equatorial region and compressional waves in the equatorial region of the plasma sheet. Our observations of Alfvénic and compressional waves during the plasma sheet thickening are consistent with this scenario, i.e., Alfvén waves were observed near the high-latitude edge of the plasma sheet, and compressional waves were seen in the inner plasma sheet. Based upon the above analysis, we propose that the Alfvénic and compressional waves in our observations are driven by the sunward quasi-period flow bursts as described by *Kepko et al.* [2001]. However, we must note that only two cases are analyzed in this study. The events in *Sundberg et al.* [2012] used to estimate the durations of flow bursts are also only from a few plasma sheet crossings. Further study with more events is necessary to confirm the conclusions in this work.

The Alfvén waves studied here could also be due to mode conversion near the equatorial region [e.g., *Keiling et al.*, 2014; *Kim et al.*, 2015]. In this model, the compressional waves generated by flow braking in the near equatorial region undergo mode conversion to Alfvén waves, which would propagate along the field line toward the nightside polar region. This scenario would also produce similar durations and spatial distribution for the Alfvénic and compressional waves in our events.

3.5. Comparison With Dipolarization Front

There have also been some observations at Earth of DFs that are accompanied by B_y fluctuations [e.g., *Sergeev et al.*, 1996; *Liu et al.*, 2013]. Detailed studies have shown that the field-aligned currents in the DF and the magnetic dip region ahead of it are in the same sense as the region-1 and region-2 FACs, respectively. However, they are one-dimensional (1-D) current sheets instead of a planar wavefront [*Liu et al.*, 2013; *Sun et al.*, 2013; *Yao et al.*, 2013]. The MVA analysis results for DFs in Table 2 of *Sundberg et al.* [2012] showed that, in almost all of their events, λ_{max} is much larger than λ_{int} and λ_{min} which are 1-D current sheets [*Sonnerup and*

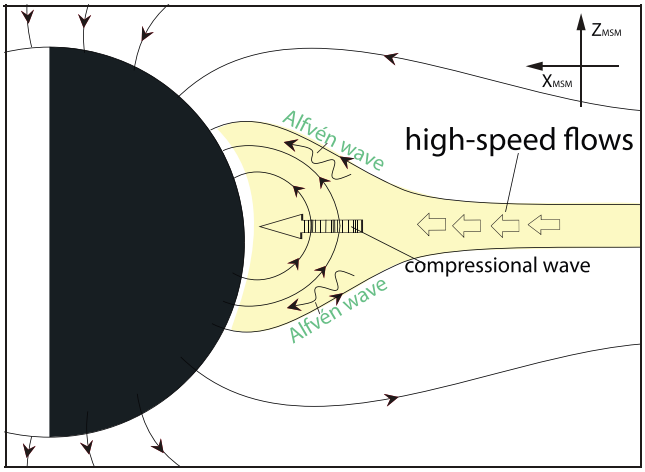

Figure 4. A schematic to illustrate the Alfvénic and compressional waves at Mercury. Alfvén wave is observed in the outer part of the plasma sheet, and the compressional wave is observed in the confined equatorial region.

Scheible, 1998]. But for B_y pulses in this study, λ_{max} is close to λ_{int} and much larger than λ_{min}, indicating that the they are planar wavefronts. We think that the B_y pulses in our events are the Alfvén wave pulses and not 1-D current sheets. The Alfvén wave pulses are most likely the carriers of field-aligned currents generated by the braking of flow bursts, which are also associated with the magnetospheric reconfiguration during the formation of the SCW.

4. Summary

In this paper, we have examined Pi2-like plasma waves occurring during substorm expansion phase in Mercury's near tail. We have analyzed pulses in the magnetic field which are the signatures of FACs generated by sunward flow bursts braking as part of the substorm dipolarization process. For both of our events, MVA analysis shows them to be circularly polarized electromagnetic waves consistent with Alfvén wave pulses. The Alfvén waves were observed when MESSENGER was located near the edge of plasma sheet at substorm onset. After MESSENGER moved into the inner plasma sheet, it then observed series of compressional waves. Both types of wave have durations of 10–20 s, suggesting that they might arise from the same source. Because of the absence of plasmasphere at Mercury, we have excluded the models associated with trapped cavity modes as an explanation for these waves. Their circular polarization also rules out their being DFs in the plasma sheet. These waves also have longer durations than the estimated travel time of Alfvén wave between the north and south hemispheres. And their wave features appear inconsistent with both standing Alfvén wave and interchange oscillations. However, because the waves were observed during rapid magnetic field line reconfiguration process, we cannot fully exclude the possibility that they are standing Alfvén waves.

The periods of the waves do appear comparable to the durations of flow bursts at Mercury inferred from DF properties, ~ 10 to 20 s, by *Sundberg et al*. [2012]. Given their association with substorm onset and duration, we speculate that these waves might be generated by the braking of quasi-periodic sunward propagating flow bursts as proposed at Earth by *Kepko et al*. [2001]. We illustrate this generation scenario of the Alfvénic and compressional waves in Figure 4. In this schematic figure, the plasma sheet is represented by the yellow region. The quasi-periodic sunward moving flow bursts are marked by the arrows in the plasma sheet along with their braking in the Mercury's near magnetotail. The FACs generated during the braking would be carried by the Alfvén waves as they propagate along the magnetic field line to the high-latitude region of Mercury's surface. The braking of flow bursts would also produce compressional waves confined to the equatorial region. However, again, we note that Alfvén waves in the high-latitude region could also be due to other mechanisms such as mode conversion near equatorial region.

The Alfvén wave pulses observed near substorm onset in this study suggest that the change of magnetospheric configuration in the near-tail plasma sheet is coupled to Mercury's nightside polar regions via the FACs carried by these Alfvén waves. Studies from Earth have shown that quasi-steady FACs begin as Alfvén waves bouncing between two hemispheres. After many bounces, the SCW forms as standing waves [e.g., *Baumjohann and Glaßmeier*, 1984; *Keiling and Takahashi*, 2011; *Kepko et al*., 2014]. The region-1 FACs driven by dayside magnetopause reconnection and the subsequent transportation of magnetic flux into the tail have been observed by MESSENGER [*Anderson et al*., 2014]. However, because of the low-lithospheric conductance at Mercury [e.g., *Verhoeven et al*., 2009; *Anderson et al*., 2014; *Jia et al*., 2015], Alfvén waves bouncing between the north and south hemispheres would likely damp before reaching a steady state and form a measurable steady state SCW.

Acknowledgments
The data used in this study were available from the Planetary Data System (PDS): http://pds.jpl.nasa.gov. The MESSENGER project is supported by the NASA Discovery Program under contracts NASW-00002 to the Carnegie Institution of Washington and NAS5-97271 to the Johns Hopkins University Applied Physics Laboratory. Wei-Jie Sun is supported by the State Scholarship Fund of Chinese Scholarship Council. This work is supported by the National Nature Science Foundation of China (grants 41474139 and 41421003) and Major Project of Chinese National Programs for Fundamental Research and Development (2012CB825603). This work was also supported by the NASA Heliophysics Supporting Research Program under grant NNX15AJ68G.

The Editor thanks Tim Yeoman and Robert Lysak for their assistance in evaluating this paper.

References

Akasofu, S. -I. (1964), The development of the auroral substorm, *Planet. Space Sci.*, *12*, 273–282.
Alexeev, I. I., E. S. Belenkaya, S. Y. Bobrovnikov, J. A. Slavin, and M. Sarantos (2008), Paraboloid model of Mercury's magnetosphere, *J. Geophys. Res.*, *113*, A12210, doi:10.1029/2008JA013368.
Alexeev, I. I., et al. (2010), Mercury's magnetospheric magnetic field after the first two MESSENGER flybys, *Icarus*, *209*(1), 23–39.
Anderson, B., M. H. Acuña, D. A. Lohr, J. Scheifele, Asseem Raval, Haje Korth, and J. A. Slavin (2007), The magnetometer instrument on MESSENGER, *Space Sci. Rev.*, *131*(1–4), 417–450.
Anderson, B. J., C. L. Johnson, H. Korth, J. A. Slavin, R. M. Winslow, R. J. Phillips, R. L. Mcnutt Jr., and S. C. Solomon (2014), Steady-state field-aligned currents at Mercury, *Geophys. Res. Lett.*, *41*, 7444–7452, doi:10.1002/2014GL061677.
Andrews, G. B., et al. (2007), The energetic particle and plasma spectrometer instrument on the MESSENGER spacecraft, *Space Sci. Rev.*, *131*(1–4), 523–556.
Baker, D. N., J. A. Simpson, and J. H. Eraker (1986), A model of impulsive acceleration and transport of energetic particles in Mercury's magnetosphere, *J. Geophys. Res.*, *91*(A8), 8742–8748, doi:10.1029/JA091iA08p08742.
Baker, D. N., T. N. Pulkkinen, V. Angelopoulos, W. Baumjohann, and R. L. McPherron (1996), Neutral line model of substorms: Past results and present view, *J. Geophys. Res.*, *101*(A6), 12,975–13,010, doi:10.1029/95JA03753.
Baumjohann, W., and K. Glaßmeier (1984), The transient response mechanism and Pi2 pulsations at substorm onset—Review and outlook, *Planet. Space Sci.*, *32*(11), 1361–1370.
Birn, J., M. Hesse, G. Haerendel, W. Baumjohann, and K. Shiokawa (1999), Flow braking and the substorm current wedge, *J. Geophys. Res.*, *104*(A9), 19,895–19,903, doi:10.1029/1999JA900173.
Chen, C. X., and R. A. Wolf (1993), Interpretation of high-speed flows in the plasma sheet, *J. Geophys. Res.*, *98*(A12), 21,409–21,419, doi:10.1029/93JA02080.
Christon, S. P., J. Feynman, and J. A. Slavin (1987), Dynamic substorm injections—Similar magnetospheric phenomena at Earth and Mercury, in *Magnetotail Physics*, edited by A. T. Y. Lui, pp. 393–400, Johns Hopkins Univ. Press, Baltimore, Md.
Gershman, D. J., J. A. Slavin, J. M. Raines, T. H. Zurbuchen, B. J. Anderson, H. Korth, D. N. Baker, and S. C. Solomon (2014), Ion kinetic properties in Mercury's pre-midnight plasma sheet, *Geophys Res Lett*, *41*, 5740–5747, doi:10.1002/2014GL060468.
Glassmeier, K. (1997), The Hermean magnetosphere and its ionosphere-magnetosphere coupling, *Planet. Space Sci.*, *45*(1), 119–125.
Glassmeier, K. (2000), Currents in Mercury's magnetosphere, in *Magnetospheric Current Systems*, edited S.-I. Ohtani et al., pp. 371–380, AGU, Washington, D. C.
Hones, E. W. (1977), Substorm processes in the magnetotail: Comments on 'On hot tenuous plasmas, fireballs, and boundary layers in the Earth's magnetotail' by L. A. Frank, K. L. Ackerson, and R. P Lepping, *J. Geophys. Res.*, *82*(35), 5633–5640, doi:10.1029/JA082i035p05633.
Hsu, T., R. L. McPherron, V. Angelopoulos, Y. Ge, H. Zhang, C. Russel, X. Chu, and J. Kissinger (2012), A statistical analysis of the association between fast plasma flows and Pi2 pulsations, *J. Geophys. Res.*, *117*, A11221, doi:10.1029/2012JA018173.
Ip, W. H. (1986), The sodium exosphere and magnetosphere of Mercury, *Geophys Res Lett*, *13*(5), 423–426, doi:10.1029/GL013i005p00423.
Jia, X., J. A. Slavin, T. I. Gombosi, L. K. S. Daldorff, G. Toth, and B. van der Holst (2015), Global MHD simulations of Mercury's magnetosphere with coupled planetary interior: Induction effect of the planetary conducting core on the global interaction, *J. Geophys. Res. Space Physics*, *120*, 4763–4775, doi:10.1002/2015JA021143.
Johnson, C. L., et al. (2012), MESSENGER observations of Mercury's magnetic field structure, *J. Geophys. Res.*, *117*, E00L14, doi:10.1029/2012JE004217.
Keiling, A. (2012), Pi2 pulsations driven by ballooning instability, *J. Geophys. Res.*, *117*, A3228, doi:10.1029/2011JA017223.
Keiling, A., and K. Takahashi (2011), Review of Pi2 models, *Space Sci. Rev.*, *161*(1–4), 63–148.
Keiling, A., et al. (2014), Magnetosphere-ionosphere coupling of global Pi2 pulsations, *J. Geophys. Res. Space Physics*, *119*, 2717–2739, doi:10.1002/2013JA019085.
Kepko, L., and M. Kivelson (1999), Generation of Pi2 pulsations by bursty bulk flows, *J. Geophys. Res.*, *104*(A11), 25,021–25,034, doi:10.1029/1999JA900361.
Kepko, L., M. G. Kivelson, and K. Yumoto (2001), Flow bursts, braking, and Pi2 pulsations, *J. Geophys. Res.*, *106*(A2), 1903–1915, doi:10.1029/2000JA000158.
Kepko, L., R. L. McPherron, O. Amm, S. Apatenkov, W. Baumjohann, J. Birn, M. Lester, R. Nakamura, T. I. Pulkkinen, and V. Sergeev (2014), Substorm current wedge revisited, *Space Sci. Rev.*, *1–46*.
Kim, E.-H., J. R. Johnson, E. Valeo, and C. K. Phillips (2015), Global modeling of ULF waves at Mercury, *Geophys. Res. Lett.*, *42*, 5147–5154, doi:10.1002/2015GL064531.
Lester, M., J. W. Hughes, and H. J. Singer (1983), Polarization patterns of Pi 2 magnetic pulsations and the substorm current wedge, *J. Geophys. Res.*, *88*(A10), 7958–7966, doi:10.1029/JA088iA10p07958.
Lin, C. A., L. C. Lee, and Y. J. Sun (1991), Observations of Pi 2 pulsations at a very low latitude (L = 1.06) station and magnetospheric cavity resonances, *J. Geophys. Res.*, *96*(A12), 21,105–21,113, doi:10.1029/91JA02029.
Liu, J., V. Angelopoulos, A. Runov, and X. Z. Zhou (2013), On the current sheets surrounding dipolarizing flux bundles in the magnetotail: The case for wedgelets, *J. Geophys. Res. Space Physics*, *118*, 2000–2020, doi:10.1002/jgra.50092.
Liu, J., V. Angelopoulos, X.-Z. Zhou, and A. Runov (2014), Magnetic flux transport by dipolarizing flux bundles, *J. Geophys. Res. Space Physics*, *119*, 909–926, doi:10.1002/2013JA019395.
Lyatsky, W., et al. (2010), Alfven wave reflection model of field-aligned currents at Mercury, *Icarus*, *209*(1), 40–45.
Maltsev, Y. P., G. V. Khazanov, and J. A. Slavin (1974), Pi-2 pulsations as a result of evolution of an Alfvén impulse originating in the ionosphere during a brightening of aurora, *Planet. Space Sci.*, *22*(11), 1519–1533.
McPherron, R. L., C. T. Russell, and M. P. Aubry (1973), Satellite studies of magnetospheric substorms on August 15, 1968: 9 Phenomenological model for substorms, *J. Geophys. Res.*, *78*(16), 3131–3149, doi:10.1029/JA078i016p03131.
Ohtani, S., M. A. Shay, and T. Mukai (2004), Temporal structure of the fast convective flow in the plasma sheet: Comparison between observations and two-fluid simulations, *J. Geophys. Res.*, *109*, A03210, doi:10.1029/2003JA010002.
Olson, J. V. (1999), Pi2 pulsations and substorm onsets: A review, *J. Geophys. Res.*, *104*(A8), 17,499–17,520, doi:10.1029/1999JA900086.
Panov, E. V., W. Baumjohann, R. Nakamura, M. V. Kubyshkina, K. H. Glassmeier, V. Angelopoulos, A. A. Petrukovich, and V. A. Sergeev (2014), Period and damping factor of Pi2 pulsations during oscillatory flow braking in the magnetotail, *J. Geophys. Res. Space Physics*, *119*, 4512–4520, doi:10.1002/2013JA019633.
Parks, G. K., et al. (2007), Solitary electromagnetic pulses detected with super-Alfvénic flows in Earth's geomagnetic tail, *Phys. Rev. Lett.*, *98*(26), 265001-1–265001-4.

Raines, J. M., et al. (2013), Distribution and compositional variations of plasma ions in Mercury's space environment: The first three Mercury years of MESSENGER observations, *J. Geophys. Res. Space Physics*, *118*, 1604–1619, doi:10.1029/2012JA018073.
Sergeev, V. A., V. Angelopoulos, J. T. Gosling, C. A. Cattell, and C. T. Russell (1996), Detection of localized, plasma-depleted flux tubes or bubbles in the midtail plasma sheet, *J. Geophys. Res.*, *101*(A5), 10,817–10,826, doi:10.1029/96JA00460.
Slavin, J. A., J. C. J. Owen, J. E. P. Connerney, and S. P. Christon (1997), Mariner 10 observations of field-aligned currents at Mercury, *Planet. Space Sci.*, *45*(1), 133–141.
Slavin, J. A., et al. (2002), Simultaneous observations of earthward flow bursts and plasmoid ejection during magnetospheric substorms, *J. Geophys. Res.*, *107*(A7), 11–13, doi:10.1029/2000JA003501.
Slavin, J. A., et al. (2010), MESSENGER observations of extreme loading and unloading of Mercury's magnetic tail, *Science*, *329*(5992), 665–668.
Slavin, J. A., et al. (2012), MESSENGER and Mariner 10 flyby observations of magnetotail structure and dynamics at Mercury, *J. Geophys. Res.*, *117*, A01215, doi:10.1029/2011JA016900.
Slavin, J., et al. (2007), MESSENGER: Exploring Mercury's magnetosphere, *Space Sci. Rev.*, *131*(1–4), 133–160.
Solomon, S., R. L. McNutt Jr., R. E. Gold, and D. L. Domingue (2007), MESSENGER mission overview, *Space Sci. Rev.*, *131*(1–4), 3–39.
Solovyev, S. I., D. G. Baishev, E. S. Barkova, and N. E. Molochushkin (2000), Pi2 magnetic pulsations as response on spatio-temporal oscillations of auroral arc current system, *Geophys Res Lett*, *27*(13), 1839–1842, doi:10.1029/2000GL000037.
Sonnerup, B. U., and M. Scheible (1998), Minimum and maximum variance analysis, in *Analysis Methods for Multi-Spacecraft Data*, edited by G. Paschmann and P. W. Daly, pp. 1850, ESA Publ., Noordwijk, Netherlands.
Southwood, D. J., and M. G. Kivelson (1990), The magnetohydrodynamic response of the magnetospheric cavity to changes in solar wind pressure, *J. Geophys. Res.*, *95*(A3), 2301–2309, doi:10.1029/JA095iA03p02301.
Southwood, D. J., and M. G. Kivelson (1991), An approximate description of field-aligned currents in a planetary magnetic field, *J. Geophys. Res.*, *96*(A1), 67–75, doi:10.1029/90JA01806.
Sun, W. J., S. Y. Fu, G. K. Parks, J. Liu, Z. H. Yao, Q. Q. Shi, Q. G. Zong, S. Y. Huang, Z. Y. Pu, and T. Xiao (2013), Field-aligned currents associated with dipolarization fronts, *Geophys Res Lett*, *40*(17), 4503–4508, doi:10.1002/grl.50902.
Sun, W. J., S. Fu, Z. Pu, G. K. Parks, J. A. Slavin, Z. Yao, Q. G. Zong, Q. Shi, D. Zhao, and Y. Cui (2014), The current system associated with the boundary of plasma bubbles, *Geophys Res Lett*, *41*, 8169–8175, doi:10.1002/2014GL062171.
Sun, W. J., et al. (2015), MESSENGER observations of magnetospheric substorm activity in Mercury's near magnetotail, *Geophys. Res. Lett.*, *42*, 3692–3699, doi:10.1002/2015GL064052.
Sundberg, T., et al. (2012), MESSENGER observations of dipolarization events in Mercury's magnetotail, *J. Geophys. Res.*, *117*, A00M03, doi:10.1029/2012JA017756.
Torrence, C., and G. P. Compo (1998), A practical guide to wavelet analysis, *Bull. Am. Meteorol. Soc.*, *79*, 61–78.
Verhoeven, O., P. Tarits, P. Vacher, A. Rivoldini, and T. Van Hoolst (2009), Composition and formation of Mercury: Constraints from future electrical conductivity measurements, *Planet. Space Sci.*, *57*, 296–305, doi:10.1016/j.pss.2008.11.015.
Wolf, R. A., C. X. Chen, and F. R. Toffoletto (2012), Thin filament simulations for Earth's plasma sheet: Interchange oscillations, *J. Geophys. Res.*, *117*, A02215, doi:10.1029/2011JA016971.
Yao, Z. H., et al. (2012), Mechanism of substorm current wedge formation: THEMIS observations, *Geophys Res Lett*, *39*, L13102, doi:10.1029/2012GL052055.
Yao, Z., et al. (2013), Current structures associated with dipolarization fronts, *J. Geophys. Res. Space Physics*, *118*, 6980–6985, doi:10.1002/2013JA019290.